NOTES AND CORRESPONDENCE

Seasonal Forecasts of North Atlantic 850-hPa Air Temperature Anomalies Using Singular Vectors

E. SÁNCHEZGÓMEZ AND M. J. ORTIZBEVIÁ

Departamento de Física, Universidad de Alcalá, Madrid, Spain

25 July 2002 and 7 May 2003

ABSTRACT

The seasonal predictability of the North Atlantic basin is assessed with the help of an empirical model. The model statistics uses the singular value decomposition of the cross-covariance matrix between the predictor (sea surface temperature anomalies) and the predictand (850-hPa air temperature anomalies) at a lag equal to the forecast lead. Three decades (1970–2000) are forecast at different lead times.

Highest skill values are found in the subtropics, near Bermuda and around the Iberian Peninsula. Skill values similar to these last can be found near the U.S. coast in autumn. In one of these regions, the model forecast sucessfully more than 50% of the variance of the unfiltered predictand field. In large regions of the domain, the skill values beat those obtained by assuming persistence. Therefore, we propose to use this model, instead of persistence, to assess the performance of the seasonal forecasts of midlatitude anomalies made with atmospheric GCMs.

1. Introduction

Though there has been considerable improvement in the atmospheric general circulation models (GCMs), they are not yet able to forecast the midlatitude atmospheric anomalies one season ahead. The bias in the simulated climatology of some of the atmospheric variables is one of the major problems. The forecast evaluation is another: the need for a number of independent predictions to quantify the forecast results (Brankovic and Palmer 2000) makes the task of producing hindcasts for several decades very expensive from the computational point of view. Although some advances have been made in those directions recently (Kanamitsu et al. 2002; Derome et al. 2002), our knowledge of the GCM's low-frequency variability is still very poor.

The statistical analysis of the observed climate provides the empirical understanding of the atmosphere–ocean interactions that is the basis of empirical forecast models. Empirical models for the Tropics (as in, e.g., Penland and Magorian 1993; Ruiz de Elvira and OrtizBeviá 1995; Penland and Matrosova 1998; Ruiz de Elvira et al. 2000) have shown useful skill values. Unfortunately, the skill of empirical forecasts for the midlatitudes, as in Shabbar and Barnston (1996), Johansson et al. (1998), and Vautard et al. (1999), is only modest. But their low computational costs and the availability of new extended datasets allow the production of forecasts for several decades, more than one season ahead. The analysis of these long empirical forecasts can assist GCM predictions, either by identifying the main sources of interannual variability within a given region or by assessing the effect of remote low-frequency signals on the forecast skill.

The empirical forecasts presented here were intended as a benchmark to assess the GCM forecast skill in the European Union–funded project Prediction of Climate Variations on Seasonal to Interannual Timescales (PROVOST). As part of this project, three state-of-art GCMs were set to simulate the atmospheric variability at 3-months lead, in a set of dynamical ''hindcast'' experiments. Meanwhile, retroactive real-time forecasts were made with the empirical model for 3 decades (1970–99), at leads ranging from 1 season to 1 yr.

Air temperature at 850 hPa (hereinafter T850) was chosen as a common target for all the PROVOST forecasts. Compared with other possible candidates, T850 has the advantages of being relevant for the North Atlantic climate, well represented in the National Centers for Environmental Prediction–National Center for Atmospheric Research (NCEP–NCAR) and ERA reanalyses, and also well connected to surface air temperature. In a first set of experiments, reported in SánchezGómez et al. (2001, 2002, hereinafter SG01 and SG02), several oceanic and atmospheric predictor fields in different

Corresponding author address: Dr. M. J. OrtizBeviá, Departamento de Física, Universidad de Alcalá, Cra. Barcelona, Km. 33.6, Alcalá de Henares, 28871 Madrid, Spain.
E-mail: mjose.ortiz@uah.es

spatial domains (several regions of the North Atlantic and/or the North Pacific) were used. In those first forecasts the variability connected to timescales below 8 months was removed from both predictor and predictand datasets in order to focus on the low frequencies. The experiment skills were acceptable (up to 56% of the variance of the filtered field, equivalent to 36% of the unfiltered one) in two regions, one in the central part of the subtropical gyre, near Bermuda, and the other over the Iberian Peninsula. Unfortunately, one of the main goals of the work was not accomplished, as it turned out that the model skill could beat the persistence skill only in a reduced region of the domain. These were our grounds for modifying the forecast model layout, leaving predictor and predictand datasets practically unfiltered (more than 90% of the raw-field anomalous variability is retained) but assessing the forecast skill on a seasonal basis, as in Johansson et al. (1998). Because of the superior performance, reported in SG01 and SG02, of the North Atlantic oceanic predictors, and in particular the SST anomalies, only SST was used as predictors.

In the following section a brief description of the predictor and predictand fields is given. In section 3, we describe the general features of the empirical forecasts method and the seasonal layout. In section 4, we present the results of the empirical forecasts experiments and analyze two cases studies. Conclusions and final remarks are given in section 5.

2. Datasets

The predictand field values, T850 anomalies, were obtained from the NCEP–NCAR reanalyses (Kalnay et al. 1996). These were monthly means in a 2.5° × 2.5° grid. The period selected is 1948–2000. As the main predictor field, we have chosen the monthly values of SST anomalies. For forecast purposes, we built an SST field for the period 1950–99 by merging the Comprehensive Ocean–Atmosphere Data Set (COADS; 1950–93) (Woodruff et al. 1987) and the Integrated Global Ocean Services System (IGOSS; 1982–99) (Reynolds and Smith 1994) dataset, as detailed in SG01. For the merged dataset, IGOSS observations have been interpolated to the COADS 2° × 2° grid. Because we built our own predictor dataset, it was possibile to issue forecasts in real time. A comparison of our predictor field with the Hadley Centre Sea Ice and Sea Surface Temperature (HadISST) dataset (Rayner et al. 2000) was presented in SG01. The spatial domain of both the T850 and SST fields is a sector of the North Atlantic (20°–90°N, 90°W–10°E) that includes large parts of the coasts of Europe, the United States, and Canada, and also the Caribbean.

In our seasonal scheme, the predictor field is separated into four sets of 3 months each, according to the seasonal phase. Each set will be called a PRE, so PRE1 encompasses the winter months (December, January, February), PRE2 the spring months (March, April, May), etc. The name has been chosen to emphasize that the PREs are not seasonal means. Nevertheless, we will see later that the covariance matrices are computed on a seasonal basis.

3. Forecast model and layout

The empirical model from which our forecasts are derived has as its core the singular value decomposition (SVD) of the lagged cross-covariance matrix between predictor and predictand fields. This statistical technique is able to isolate pairs of patterns from both predictor and predictand fields that maximize their covariance under orthogonality assumptions.

For a forecast at a given lead l, issued from a certain PRE, we first compute the anomalies of the predictor $y(t)$ and predictand $z(t)$ fields (by substracting their monthly mean) and then calculate the lagged cross-covariance matrix C between both, for all the months included in the PRE:

$$C = \langle z(t)y^T(t - l)\rangle = \sum_{i=1+l}^{t_p} z_i y_{i-l}^T, \tag{1}$$

where t_p is the time of the forecast start. By its SVD, C can be written:

$$C = \sum_{k=1}^{N} w_k \mathbf{u}_k \mathbf{v}_k^T, \tag{2}$$

where $\mathbf{u}_k$ and $\mathbf{v}_k$ are the singular vectors associated with the predictand and predictor fields, respectively, and w_k is the k-th singular value of C.

The SVD yields pairs of seasonal patterns that isolate coupled features where the time evolution of the predictor field must theoretically precede the time evolution of the predictand field at the lead time considered. Furthermore, the patterns can be ordered decreasingly by their corresponding singular value, which gives us the amount of the coupled covariance explained at lag l. A reduction of the number of degrees of freedom is then straightforward (Bretherton et al. 1992; Navarra 1993).

Through the projection of each field onto the corresponding vector, we obtain empirical coefficients for the predictand $[a_k(t)]$ and predictor $[b_k(t)]$ fields. The time coefficients represent the temporal evolution of the singular pattern k. The forecast value $\hat{z}_q(t)$ at the time $t_p + l$ is built by an expansion in which the predictor time coefficient $b_k(t - l)$ is weighted by the singular vector of the predictand field:

$$\hat{z}_q(t_p) = \sum_{k=1}^{q} c_k b_k(t_p - l)\mathbf{u}_k, \tag{3}$$

where c_k is the empirical coefficient relating the temporal evolution of $a_k(t)$ and $b_k(t - l)$.

Likewise, the predictand field $z_q(t_p)$ is given in the form

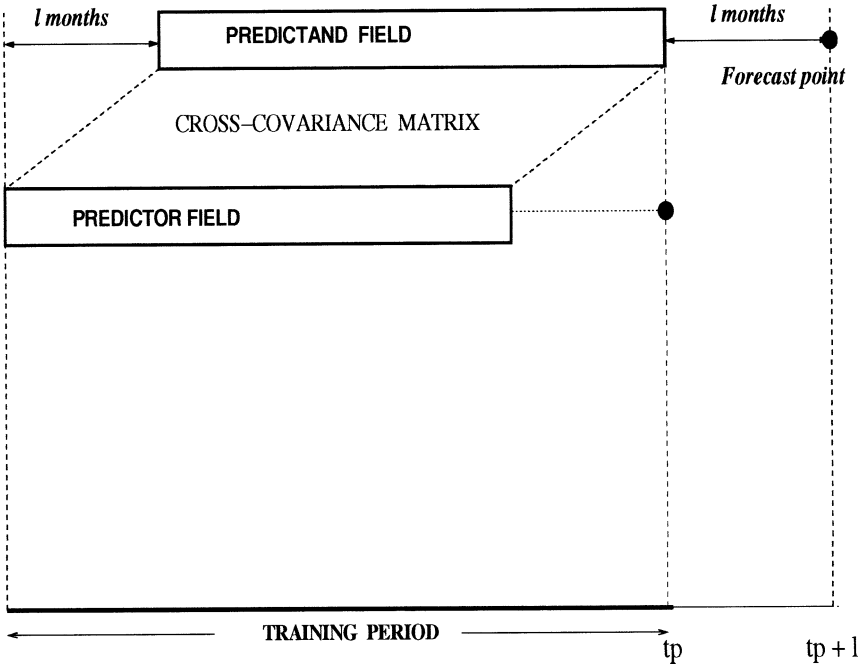

FIG. 1. Illustrative scheme of the forecast procedure. Only the information from the training period is used to produce the forecasts.

$$z_q(t_p) = \sum_{k=1}^{q} a_k(t_p)\mathbf{u}_k. \quad (4)$$

By truncation, we retain only the first singular modes q that together are supposed to explain most of the joint variability of both fields (the total number of modes is N). As the time series projected on these seasonal singular vectors is formed with monthly values, we obtain a monthly forecast, whose skill is nevertheless assessed on a seasonal basis. The procedure followed to build the empirical model is represented in Fig. 1. The seasonal forecast layout, similar to the one used in the analysis of Czaja and Frankignoul (1999), is shown schematically in Fig. 2.

In the empirical forecasts both the predictand and predictor fields are divided in two segments: training sample and validation period. For one forecast l seasons ahead, starting at PRE i, year j, the training sample is formed with the observations in all the years preceding the start of the forecasts. Predictions are assessed against the anomalies computed from the validation period that begins with the dataset (1948) and includes the forecast time interval. The procedure followed here has been designed to produce a real forecast, not a hindcast, since only the ''past'' is used to make a prediction. Nevertheless, as the validation value is known beforehand, these have been called ''retroactive real-time forecasts'' (Barnston et al. 1994).

Each of the months in the four predictor sets separately forecasts one of the months in a season of the predictand field. Figure 2 schematizes the sequence: as the lead time varies (from 3 to 12 months), the PRE predicts the predictand season. The forecast experiments are systematically repeated for the four PRE. To assess the skill at a certain lag l of a PRE, the three forecasts performed at lead l with this PRE are taken into account. This reduces drastically the training sample size. In order to avoid the problems derived from a short training interval, this sample size is gradually increased, taking into account the corresponding PRE in all the years previous to the start of the forecast. Finally, the skill of the forecasts is assessed through the correlation between the predictand field (reconstructed with q patterns) and the forecast field.

Field significance

As the number of spatial patterns used to forecast is not small, the problem of an artificial skill obtained by overfitting has to be considered. The levels of the artificial skill are estimated using a bootstrap procedure (Efron and Tibshirani 1993). Following Yuval (2001), a large number (100) of artificial predictor and predictand fields are obtained by random sampling of the original ones. The time series of the predictand and predictor fields is split into several segments, or blocks, of the same length. Then the replicas are built by the random reorganization of the segments. The point where the division starts is changed for each realization. To ensure statistical independence, the blocks' lengths are selected as the largest values in the decorrelation time, as defined in Livezey and Chen (1983). The number of times the real skill is under the simulated values provides the significance level. For the evaluation of the empirical forecasts, persis-

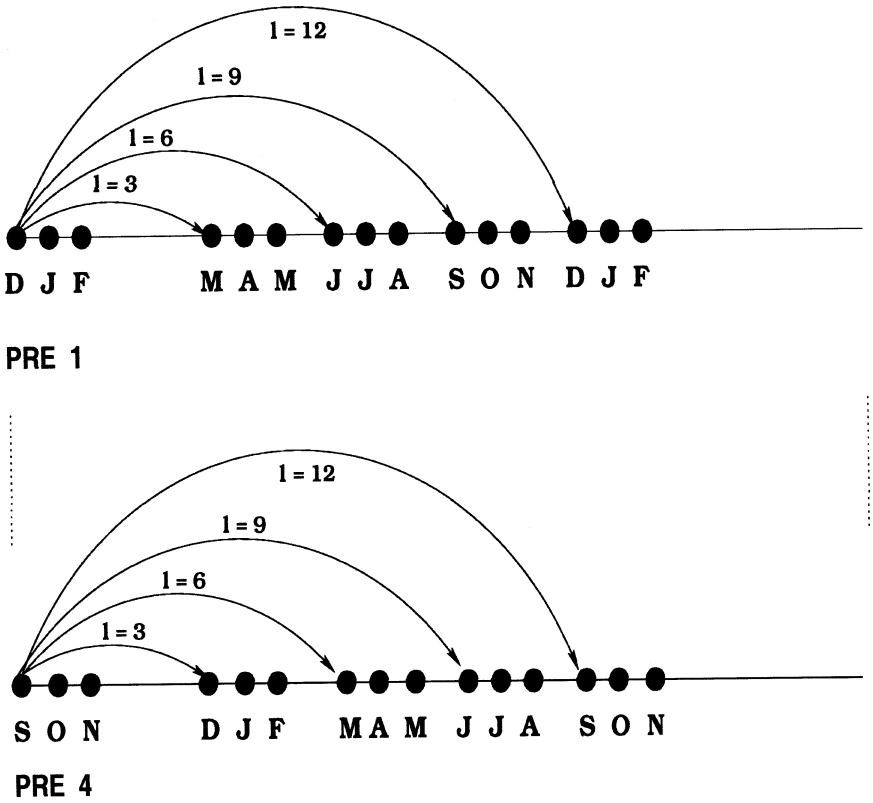

FIG. 2. The sequence of the forecast procedure for the seasonal scheme. Given a predictor field, the target season changes as the forecast lead time increases.

tence-based predictions have been a common reference in previous forecasts and are also used here.

4. Forecast experiments

Previous to the forecasting, the optimal number of patterns to be used in the reconstruction and forecast of the predictand field has to be decided. The choice made here is partially based on the percentage of cumulative variance explained. We have also taken into account, as in SG01 and SG02, how well the counterpart in the T850 field of the North Atlantic Oscillation (NAO), the dominant climatic signal in this region, is represented in the reconstructed field. From this study, it is inferred that the optimal number of patterns to be retained is 20 (which accounts for more than 90% of the variance of the unfiltered field).

a. Forecast skill of North Atlantic T850 anomalies

Seasonal forecasts of the T850 anomalies at different lead times were made, following the scheme represented in Fig. 2. The forecasted period goes from 1970 through 2000. The forecasts have been made from 3 (spring is the targeted season) to 12 (in this case it is winter) months ahead. In the forecasts at 3- and 6-months lead times, the highest values of the skill are found in two regions. In one, located in the subtropics, the skill levels exceed a value of 0.5 when summer is the target season. In the forecasts for summer and autumn, there is a secondary maximum over southern Europe. In this last case, the values are similar to those along the U.S. coast. When the winter SST are used to forecast the following winter, values of the skill fall significantly. For reasons of space, we will present only the skill averages to the regions depicted in Fig. 3. The selection of these regions is based on the differences found in the skill levels mentioned above. The skill of the PRE1 forecast is represented in this way in Fig. 4 (top). Our forecasts do achieve a significant improvement against persistence, as can be observed in Fig. 5.

b. Seasonal dependence of forecast skill

Seasonal changes in the skill that were barely noticeable in SG01 because of the time filtering can be studied here. We give only a brief account of this study. For region I, the skill is higher in summer, notwithstanding the lead time. Skill values are not statistically significant at the 95% level in regions III and IV. In regions II (near the Iberian Peninsula) and V (along the U.S. coast), there is a maximum of skill in summer and autumn. In general, for the five regions in the domain, the skill decreases as the forecast lead time increases.

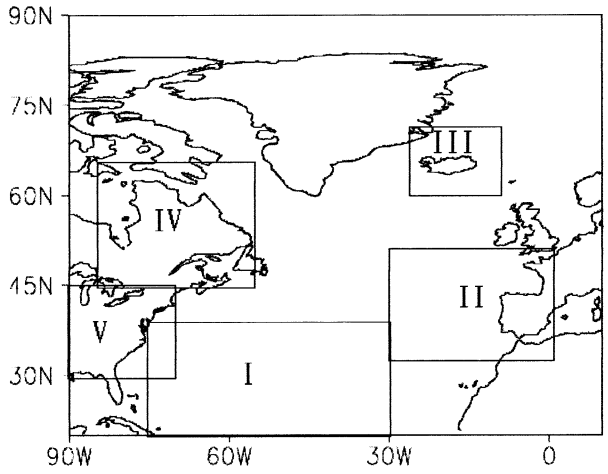

FIG. 3. The regions in which the values of the skill have been averaged: region I (20°–40°N, 75°–30°W), region II (35°–50°N, 30°W–0°), region III (60°–70°N, 25°–10°W), region IV (45°–65°N, 85°–55°W), and region V (30°–45°N, 90°–70°W).

However, there are some situations in which the skill shows relative insensitivity to the forecast lead time, as for instance in the case of region I for the summer season. This fact is encouraging for long-lead forecast purposes.

c. *Cross-validation experiments*

Decadal timescales are known to play an important part in the anomalous variability of the midlatitudes observations. Until recently, the record length of the midlatitudes observations was at the most 40 years, and was at very sparsely distributed stations. Therefore, most of the midlatitude empirical forecast models mentioned in the introduction used cross-validation experiments to assess their skills. In most of the cross-validation experiments, as is the case in those presented here, only the target year is withheld from the training sample. This technique can provide representative results with respect to real forecasts, although, as pointed out in Barnston et al. (1994), there is a danger of skill inflation because of the existence of important interannual autocorrelation in the data.

On the other hand, the ENSO empirical forecasts presented in the forecast forum of the *Climate Diagnostic Bulletin* (http://www.cpc.ncep.noaa.gov) have shown, with the same limitations in the training sample length, a considerable skill compared with those made with the more sophisticated coupled GCM. Encouraged by this example, we have chosen to make retroactive real-time forecasts. Nevertheless, cross-validation experiments for all the PREs have also been included in the present study. From these, we show in Fig. 4 the cross-validation skill values (bottom) of the four regions monitored for the PRE1 experiments (predictor in winter) to be compared with those of the retroactive real-time forecasts (top) in the same conditions. With the present forecast

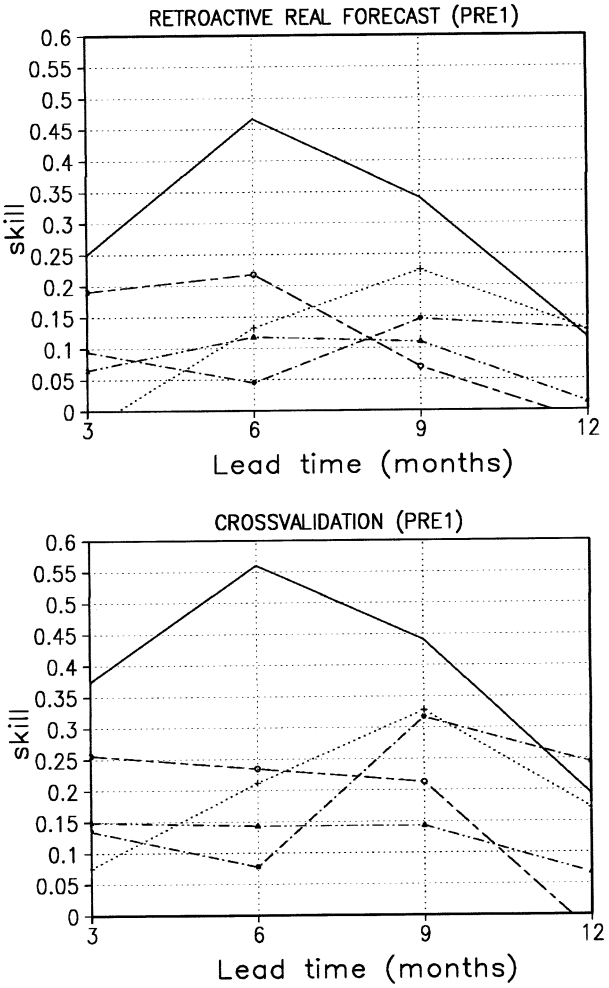

FIG. 4. Comparison of the skill values obtained by the retroactive real-time forecasts (top) against those of the crossvalidation forecasts (bottom). The values of the skill have been averaged over the five regions defined in Fig. 3: region I (solid), region II (dash), region III (dot–dash), region IV (dot–dot–dash), and region V (dots).

scheme, the skill inflation seems less important than in the case of the filtered forecasts presented in SG01.

d. *Two case studies: Winter of 1976 and summer of 1994*

As in SG01, the model performance is illustrated in two particular situations where sizeable and persistent air temperature anomalies were observed: the winter of 1976 and the summer of 1994. The forecasts in Fig. 6 are compared with their counterparts in SG01 (Figs. 10,11 there). The left-hand column in Fig. 6 represents (a) the predictand field, (b) the forecast, and (c) the predictor field one year in advance for T850 anomalies in winter 1976. The only difference between this predictor field and the one in SG01 is the magnitude of the SST anomalies: the highest positive anomalies south of Newfoundland were 0.5 K in SG01 and reach 1 K

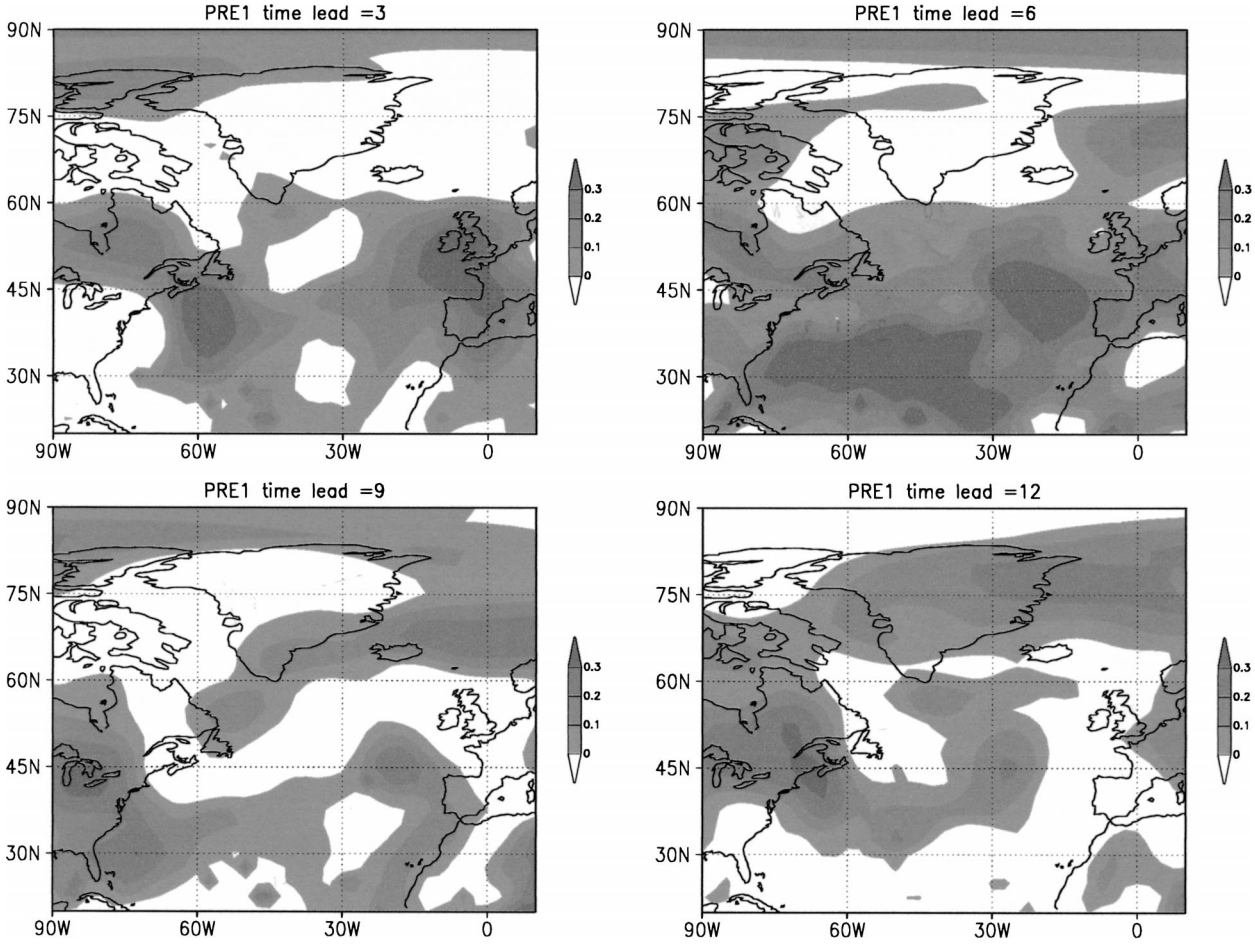

FIG. 5. Comparison with the persistence forecasts. The difference between the skill of the model and the skill obtained assuming persistence has been computed. The shaded region indicates where the model beats the persistence.

here. Differences in the forecast field are important. Forecasts in SG01 were only able to reproduce the positive atmospheric signal south of Newfoundland, missing the warm anomaly in northern Europe that is captured here. There is also a better estimation of the magnitude of the atmospheric anomalies.

Likewise, the right column in Fig. 6 represents (d) the predictand field, (e) the forecast, and (f) the predictor field one year in advance in the case of the summer of 1994. The SST pattern is characterized here by a warming in the central part of the subtropical Atlantic and northwest Europe and a cooling adjacent to the North American coast and over the north of the domain. In SG01 the model was succesful at predicting the sign of the positive T850 anomalies over the North American coasts and the Iberian Peninsula. But the forecast again improves, since the magnitude of the anomalies (even the negative ones) is better captured here.

e. Origin of the forecast skill

The origin of the forecast skill is investigated through the analysis of the singular vectors used to forecast, among which the first singular patterns play a leading part. The oceanic pattern remains almost invariant to the forecast lead. It represents a bipolar structure between the region east of North America, where the subtropical and subpolar gyres converge, and the southern part of the subtropical gyre (the region of Bermuda). For lead times from 3 to 6 months, highest loadings in the oceanic pattern are for the coast of Iberia and the Bermuda region. However, this center of action weakens for lead times above 9 months. Some of the features of this oceanic predictor can be distinguished in the oceanic forcing pattern used to forecast the 1994 summer (Fig. 6f).

The predictand pattern is more sensitive to the forecast lead time and thus depends on the target season. For all of the cases studied, the highest loadings correspond to the subtropical region, where the best values of the skill have been found. The skill captures the atmospheric response along the eastern coast of the basin (North America) at 3-months lead time, while at greater leads there is an increase in skill over Iberia, North Africa, and the Mediterranean when the target seasons are summer (6-months lead time) and autumn (9-months lead time).

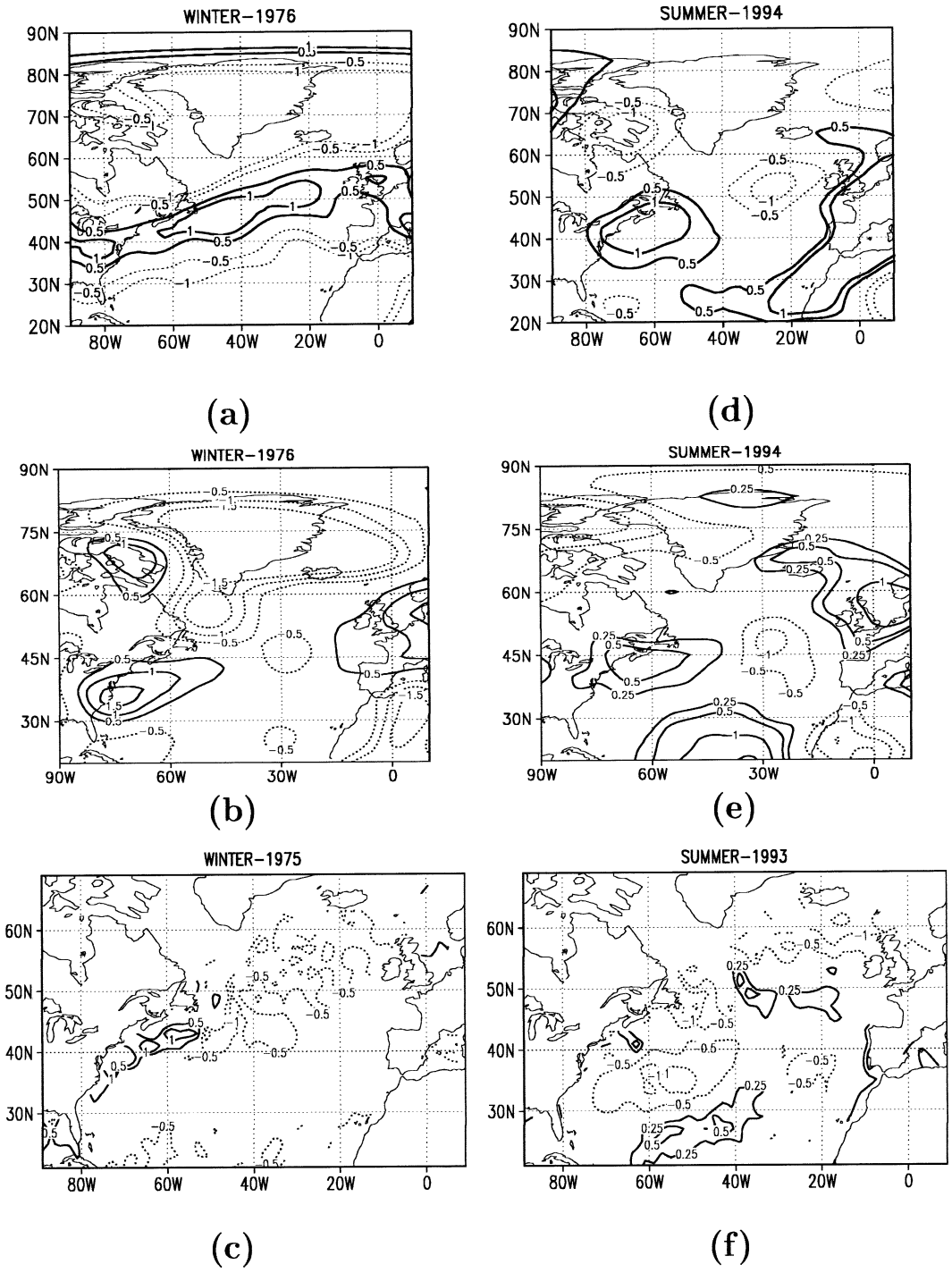

FIG. 6. Two case studies: the cold winter of 1976 (left-hand side) and the warm summer of 1994 (right-hand side). The (c), (f) 12-months-ahead forecasts are shown against (a), (d) the air temperature (K) and (b), (e) the SST observations (K).

5. Summary and conclusions

This study is based on the hypothesis of Bjerkness (1964) that the red-noise variability in the ocean, which is forced by the atmosphere at short timescales, may in turn induce or alter atmospheric anomalies. We study the seasonal predictability of the North Atlantic, using an empirical model based on the SVD of the seasonal cross-covariance matrix computed between the predictand field (850-hPa air temperature anomalies) and the

predictor field (SST anomalies). The causal relationship between the atmosphere and the ocean is captured by computing the seasonal cross-covariance matrix at a lag corresponding to the forecast lead.

The basic feature of the empirical model used here has been already introduced in previous papers (SG01; SG02). There the empirical model was applied to filtered fields (roughly 50% of the variance of the unfiltered field was retained), while here the fields have been only slightly smoothed (more than 90% retained). In the present study, we find that the predictability is mainly confined to the subtropical region around Bermuda. During the summer and autumn, the predictability spreads over the Iberian Peninsula and the Mediterranean. Some of these results appear also in SG01, but here the amount of variance explained is in some cases above 50% of the total variance of the field, while there it explained barely 36%. Here, there is also a skill improvement (with respect to the SG01 forecasts) in a region along the U.S. coast in autumn, with values similar to the ones found near the Iberian Peninsula. This improvement is connected to the inclusion of the timescales between 6 and 9 months.

The origin of the forecast skill can be traced back to the relationship between an oceanic dipole pattern and the atmospheric variability. One of the centers of action of this pattern is located in a region to the east of Newfoundland where the subtropical and the subpolar gyres converge and the other is located in the southern part of the subtropical gyre, near Bermuda.

The skill dependence on the annual cycle is on the target rather than on the predictor season. The predictability increases when summer is the target season. This fact is in good agreement with the remarks by Brankovic et al. (1994) and also by Schubert et al. (2001). During the summer, the internal chaotic dynamics of the atmosphere weakens, the predictability is enhanced, and the extratropical lower-boundary forcing plays a more relevant part in the dynamics.

The new version of the model achieves a significant improvement of its skill, as compared with the persistence skill, over most of the domain. In this sense, we present here an improved benchmark to the forecast of atmospheric anomalies made with atmospheric GCMs.

Acknowledgments. Thanks are due to F. Alvarez for his help editing this manuscript. We thank also the two anonymous reviewers for their comments. This work was supported by the European Union under Contracts CT95-0109 (PROVOST) and CT98-0714 (SINTEX).

REFERENCES

Barnston, A. G., and Coauthors, 1994: Long-lead seasonal forecasts—Where do we stand? *Bull. Amer. Meteor. Soc.,* **75,** 2097–2114.

Bjerkness, J., 1964: Atlantic air–sea interaction. *Advances in Geophysics,* Vol. 10, Academic Press, 1–82.

Brankovic, C., and T. N. Palmer, 2000: Seasonal skill and predictability of ECMWF PROVOST ensembles. *Quart. J. Roy. Meteor. Soc.,* **126,** 2035–2067.

——, ——, and L. Ferranti, 1994: Predictability of seasonal atmospheric variations. *J. Climate,* **7,** 217–237.

Bretherton, C. S., C. Smith, and J. M. Wallace, 1992: An intercomparison of methods for finding coupled patterns in climate data. *J. Climate,* **5,** 541–560.

Czaja, A., and C. Frankignoul, 1999: Influence of North Atlantic SST on the atmospheric circulation. *Geophys. Res. Lett.,* **26,** 2969–2972.

Derome, J., and Coauthors, 2002: Seasonal predictions based on two dynamical models. *Atmos.–Ocean,* **39,** 485–501.

Efron, B., and J. R. Tibshirani, 1993: *An Introduction to the Bootstrap.* Chapman and Hall, 436 pp.

Johansson, A., A. Barnston, A. Saha, and H. Van den Dool, 1998: On the level and origin of seasonal variability forecast skill in northern Europe. *J. Atmos. Sci.,* **55,** 103–127.

Kalnay, E., and Coauthors, 1996: The NCEP/NCAR 40-Year Reanalysis Project. *Bull. Amer. Meteor. Soc.,* **77,** 437–471.

Kanamitsu, M., and Coauthors, 2002: NCEP dynamical seasonal forecast system 2000. *Bull. Amer. Meteor. Soc.,* **83,** 1019–1032.

Livezey, R. E., and W. Y. Chen, 1983: Statistical field significance and its determination by Monte Carlo techniques. *Mon. Wea. Rev.,* **111,** 46–58.

Navarra, A., 1993: A new set of orthonormal modes for linearized meteorological problems. *J. Atmos. Sci.,* **50,** 2569–2583.

Penland, C., and T. Magorian, 1993: Prediction of Niño 3 sea surface temperatures using linear inverse modeling. *J. Climate,* **6,** 1067–1076.

——, and L. Matrosova, 1998: Prediction of tropical Atlantic sea surface temperature using linear inverse modeling. *J. Climate,* **11,** 483–496.

Rayner, N. A., D. E. Parker, P. Frich, E. B. Horton, C. K. Folland, and L. V. Alexander, 2000: SST and sea-ice fields for ERA-40. *Proc. Second World Climate Research Program Int. Conf. on Reanalysis,* Reading, United Kingdom, World Meteorological Organization, WMO/TD-985, WCRP-109, 18–22.

Reynolds, R. W., and T. M. Smith, 1994: Improved sea surface temperature analyses. *J. Climate,* **7,** 929–948.

Ruiz de Elvira, A., and M. J. OrtizBeviá, 1995: Application of statistical techniques to the analysis and prediction of ENSO. *Dyn. Atmos. Oceans,* **22,** 91–114.

——, ——, and W. CabosNarvaez, 2000: Empirical predictions of tropical Atlantic SST anomalies. *Quart. J. Roy. Meteor. Soc.,* **126,** 2199–2210.

SánchezGómez, E., F. Alvarez, and M. J. OrtizBeviá, 2001: Empirical prediction of 850 hPa North Atlantic air temperature anomalies. *Quart. J. Roy. Meteor. Soc.,* **127,** 2761–2786.

——, W. CabosNarváez, and M. J. OrtizBeviá, 2002: Sea ice anomalies as long range predictors of atmospheric conditions in the North Atlantic basin. *Tellus,* **54A,** 245–259.

Schubert, S. D., M. J. Suarez, Y. Chang, and G. Branstator, 2001: The impact of ENSO on extratropical low-frequency noise in seasonal forecasts. *J. Climate,* **14,** 2351–2365.

Shabbar, A., and A. G. Barnston, 1996: Skill of seasonal climate forecasts in Canada using canonical correlation analysis. *Mon. Wea. Rev.,* **124,** 859–881.

Vautard, R., G. Plaut, R. Wang, and G. Brunet, 1999: Seasonal prediction of North America surface air temperature using space–time principal components. *J. Climate,* **12,** 380–394.

Woodruff, S. D., E. J. Slutz, R. L. Jenne, and P. M. Steurer, 1987: A comprehensive ocean–atmosphere data set. *Bull. Amer. Meteor. Soc.,* **68,** 1239–1250.

Yuval, N., 2001: Enhancement and error estimation of neural network prediction of Niño-3.4 SST anomalies. *J. Climate,* **14,** 2150–2163.